# Ionospheric delay estimation using Galileo E5 signals only

Olivier Julien, Jean-Luc Issler, Laurent Lestarquit

# Ionospheric Delay Estimation Using Galileo E5 Signals Only

Olivier Julien, *Ecole Nationale de l'Aviation Civile, Toulouse, France*
Jean-Luc Issler, Laurent Lestarquit, *Centre National d'Etudes Spatiales, Toulouse, France*

## BIOGRAPHY

**Olivier Julien** is a the head of the SIGnal processing and NAVigation (SIGNAV) research group of the TELECOM laboratory of ENAC (Ecole Nationale de l'Aviation Civile – French Civil Aviation University), Toulouse, France. His research interests are GNSS receiver design, GNSS multipath and interference mitigation and GNSS interoperability. He received his engineer degree in 2001 in digital communications from ENAC and his PhD in 2005 from the Department of Geomatics Engineering of the University of Calgary, Canada.

**Laurent Lestarquit** is a navigation signal expert at the CNES Transmission Technique and Signal Processing department (TT). He was a member of the Galileo Signal Task Force (GSTF) and contributed to the definition of the Galileo signal and provided support to the 2004 US-EU agreement of navigation system. He invented the constant envelope 4-code ALT-BOC modulation and is one of the CBOC inventors.

**Jean-Luc Issler** is head of the Instrumentation Telemetry and Propagation department of the CNES Radio Frequency sub-directorate since august 2009. He is one of the CBOC inventors, and proposed the GALILEO E5 signal using the ALTBOC 8-PSK invention. He graduated first from ESEO. He received the Astronautic Prize of AAAF (French aeronautical and space association) in 2004, and the EADS Science and Engineering prize, delivered in 2008 by the French Academy of Sciences, for his work on GNSS frequencies and modulations, and spaceborne RF equipments.

## ABSTRACT

This article presents an analysis of a ionospheric delay estimator based on dual-frequency GNSS signals that are located in very close frequency bands. The target area is mid-latitude locations, such as Europe, where a fairly simple local ionospheric delay model can be used to simplify the estimator. A total of 8 local ionospheric model are tested in different European locations under different levels of ionosphere activities (high to very high). The simulations assume that the NeQuick model is representative of the true ionospheric delay.

The results show that different local ionospheric delay models can be used depending upon the location of the user: from very simple ones in Northern Europe where the ionospheric delay does not vary greatly with the ionosphere pierce point location to more advanced ones in Southern and middle Europe where the ionospheric delay can vary significantly with the pierce point location. It also shows that it can provide very interesting results in terms of ionospheric delay estimation accuracy: as an example, the ionospheric delay estimation error standard deviation at L1 in Toulouse, France, is below 50cm for a very active ionosphere (within the top 7.5% over 1931-2001).

## INTRODUCTION

Future Galileo open signals, E5 (E5A/E5B) and E1 OS, were designed so that they can bring significant improvements to most of the users compared to the current GPS L1 C/A signal performances. Receivers will thus be able to track the different signals with a lower tracking noise and a lower multipath susceptibility, and an increased resistance to interferers, consequently providing cleaner code and phase pseudorange measurements. This enhancement was obtained thanks to, among others, the use of higher code chipping rates (10.23 MHz for E5A and E5B), innovative modulations (BOC, ALTBOC, MBOC) and the use of a pilot channel in parallel with the traditional data channel.

The use of the 3 Galileo open signals together can bring further obvious improvements such as (1) a more accurate and robust ionospheric delay estimation, (2) improved ambiguity resolution performances (in terms of success rate and time to fix), (3) potential tropospheric delay estimation, and (4) frequency diversity against potential intentional or unintentional interference. The concept of frequency diversity has been introduced in [Shau-Shiun Jan, 2002]. These different points were backed up by many different investigations and papers from

different user community needing high precision and reliable positioning, showing a great interest in, for instance, a triple-frequency Galileo (and GPS) receiver.

Based on this triple frequency baseline, it is however important when it comes to sensitive applications, to consider degraded modes since it might impact the expected behavior of the receiver. A typical example is the loss of one frequency and it is thus important for a triple-frequency Galileo receiver to consider the loss of any of the E5A, E5B and E1 signal and its consequence on required performances.

This article specifically focuses on the event of the loss of the Galileo E1 OS signal. This situation is of particular interest because it means that the receiver is left with measurements coming exclusively from E5A and E5B signals, which are spectrally very close and thus not ideal for high precision positioning. Many different figures of merit are to be investigated in this degraded mode scheme to fully assess how the receiver can cope without significantly losing any of its performance. However, this article will only focus on the ionospheric delay estimation using only E5A and/or E5B signals.

The motivation behind this investigation is to show that for a triple frequency Galileo receiver, whatever the jammed band, it is always possible to estimate accurately the ionospheric delay affecting pseudorange measurements and thus keep the high accuracy positioning ability of the receiver. Moreover, an extension of this conclusion is the potential use of the E5 band alone for precise positioning applications [Issler et al, 2004].

This document is the follow-on of a previous investigation realized in 2009 [Julien et al, 2009] that investigated the use of an ionospheric delay estimation process based on a Kalman Filter (KF). This KF was based on code and phase geometry free combinations (using Galileo E5A and E5B measurements), jointly with a simplified local model of the Vertical Total Electron Content (VTEC) to represent the ionospheric delay of any visible satellites. This simplified VTEC model was based on the estimation of the VTEC at the ionosphere pierce point relying on the estimation of 3 parameters:

- the estimated VTEC at the user zenith
- the estimated latitude and longitude VTEC gradients

The initial results were promising since the ionospheric delay estimation error standard deviation was at the decimeter-level even for low elevation satellites. However, these results were obtained using simulations assuming that the true ionospheric delays could be represented using the Klobuchar model. The objective of this investigation is thus twofold:

- to better model the true ionospheric delay by using a more representative ionosphere model than the Klobuchar model. It was decide to use the NeQuick model.
- to improve the ionospheric delay estimation technique and test it using new local VTEC models. 7 local ionosphere models (based on up to 5 states to estimate) have been tested in the KF to improve the estimation process.

This article is thus organized as follows:

- section 2 presents the Galileo E5 signals and the observables' model
- section 3 presents the reference ionospheric delay estimation techniques introduced in [Julien et al, 2009]
- section 4 presents an analysis of the local VTEC variations based on the NeQuick model and introduced the proposed local VTEC models that will be investigated
- section 5 presents the simulation tools and estimation filter settings.
- section 6 presents test results based on the reference estimation filter
- section 7 presents test results for all the considered local VTEC models
- section 8 presents the conclusions and future work.

## DESCRIPTION OF GALILEO E5 SIGNALS AND ASSOCIATED OBSERVABLE MODELS

### Presentation of the Galileo E5 Signal

The Galileo E5 signals are part of the E5 band ([1164-1215 MHz] that is the largest RadioNavigation Satellite System (RNSS) band [European Union, 2010]. It is also an Aeronautical RadioNavigation Service (ARNS) band, thus protected by ITU, but with no exclusivity to RNSS. This means that any system broadcasting within this band will have to cope with the existing non-RNSS services already present in this band. In particular, systems using strong pulsed signals, such as Distance Measuring Equipments (DME), and TACtical Air Navigation (TACAN) are deployed in this band [RTCA, 2004; Bastide, 2004].

The Galileo E5 signal has 2 components:

- The E5a signal is transmitted in the frequency band [1164 MHz – 1191.795 MHz] and centered on $f_{E5a}$=1176.45 MHz. It will fully support the Galileo Open Service (OS) and will support the Safety of Life (SoL) service through its ranging function. It is composed of a data and pilot channel with equal power. The data channel broadcasts the F/NAV message (corresponding to the OS) with a symbol rate of 50 sps. Since the useful data is encoded using a convolutional code with a constraint ½, the actual data bit rate is 25 bps. Galileo E5a is Quadra-Phase Shift Keying (QPSK)-modulated and uses a 10230-chip long spreading code with a chipping rate $f_c$ of 10.23 MHz. This means that it is a wide-band signal that will exhibit excellent resistance towards thermal, multipath and narrow-band interference compared to the currently available GPS C/A signal. It is also worth noting that the Galileo E5a signal will overlap the GPS L5 signal, which has similar signal characteristics. It means that it will likely be part of GPS/Galileo receivers using the E5a/L5 frequency band.
- The E5b signal is transmitted in the frequency band [1191.795 MHz – 1215 MHz], centered on $f_{E5b}$=1207.14 MHz. The Galileo E5b signal will support the OS, the SoL full service (ranging and integrity functions) and the Commercial Service (CS). It is composed of data and a pilot channels with equal power. The data channel broadcasts the I/NAV message (corresponding to the SoL service) with a symbol rate of 250 sps This means a useful data bit rate of 125 bps due to the convolutional encoding with a constraint 1/2. Galileo E5b uses a 10230-chip long spreading code with a chipping rate $f_c$ of 10.23 MHz. Although the Galileo E5b does not coincide spectrally with any planned GPS signal, it has the same frequency and modulation as the future COMPASS B2 signal, which might be interoperable with Galileo E5b, and is very close to the future GLONASS L3 signal.

It can be seen that Galileo E5a and Galileo E5b are present in adjacent bands. In order to take advantage of that, the 2 signals are transmitted coherently using an ALTBOC(15,10) modulation [Lestarquit et al., 2008]. The whole Galileo E5 signal is thus an extra wide-band signal (more than 50 MHz wide) that can be received:

- as a whole: this means that the user can process an extra-wide band signal for positioning, thus enjoying pseudorange measurements that are the most resistant GNSS signals towards thermal noise, multipath and narrow-band interference [Simski et al, 2006].
- separately: in this case, the user does not require a receiver with an extra-wide bandwidth, thus reducing the complexity of the receiver. Note that a dual frequency E5a/E5b receiver can process in parallel both signals, thus obtaining measurements from 2 wide-band signals that were generated based on the same satellite payload module (same filter with excellent stability over the E5 band, same HPA) at 2 different frequencies.

Compared to the Galileo E1 OS, and to a larger extend GPS L1 C/A, the Galileo E5a and E5b signals will provide enhanced tracking capabilities, and thus are very promising for precise positioning applications. Moreover, [Galileo SIS ICD, 2008] specifies that both Galileo E5a and E5b signals should be received with a minimum power 2 dB above the Galileo E1 OS. This also means a better performance in case of signal obstruction.

The Galileo E5 signal performances were presented in [Julien et al, 2009] and will not be detailed in here. It is still worth mentioning that:

- the coherent code tracking performance (against thermal noise, multipath and interference) of the Galileo E5 signal is extremely good compared to any other GNSS signals due to its very wide bandwidth
- the coherent code tracking of the Galileo E5a and E5b is equivalent to the code tracking performance of the GPS L5.

**Observable Model**

Let us denote $P_X^{S_Y}$ and $\varphi_X^{S_Y}$ the code and carrier phase pseudorange measurements from satellite $S_Y$ at frequency $X$. Their usual model is provided by:

$$\begin{aligned} P_X^{S_Y}(k) = {} & \rho^{S_Y}(k) + c\left(dT^{S_Y}(k) - dt^{S_Y}(k)\right) \\ & + T^{S_Y}(k) + I_X^{S_Y}(k) \\ & + MP_{P,X}^{S_Y}(k) + n_{P,X}^{S_Y}(k) \\ & + b_{P,X}^{S_Y}(k) \end{aligned} \quad \text{Eq. 1}$$

$$\begin{aligned} \varphi_X^{S_Y}(k) = {} & \rho^{S_Y}(k) + c\left(dT^{S_Y}(k) - dt^{S_Y}(k)\right) \\ & + T^{S_Y}(k) - I_X^{S_Y}(k) \\ & + MP_{\varphi,X}^{S_Y}(k) + n_{\varphi,X}^{S_Y}(k) \\ & + b_{\varphi,X}^{S_Y}(k) + \lambda_X A_X^{S_Y} \end{aligned} \quad \text{Eq. 2}$$

where

- the superscript $S_Y$ refers to the satellite $Y$,
- $\rho$ represents the true satellite-receiver range,

- $dT$ represents the satellite clock bias,
- $dt$ represents the receiver clock bias,
- $T$ represents the tropospheric delay,
- $I_X$ represents the ionospheric delay at freq. $X$,
- $MP_P$ and $MP_\varphi$ represent the errors due to multipath on the code and phase pseudoranges,
- $n_P$ and $n_\varphi$ represent the error due to thermal noise on the code and phase pseudoranges,
- $b_{P,X}^{S_Y}$ and $b_{\varphi,X}^{S_Y}$ represent the satellite+receiver code and phase biases at frequency $X$.
- $A_X$ represents the carrier phase ambiguity at frequency $X$,
- $\lambda_X$ represents the wavelength of the carrier $X$.

In order to gather the elements of Eq. 1 and Eq. 2 that are common to the different frequencies and observables of satellite $S_Y$, they can be re-written as:

$$P_X^{S_Y}(k) = D^{S_Y}(k) + I_X^{S_Y}(k) + MP_{P,X}^{S_Y}(k) + n_{P,X}^{S_Y}(k) + b_{P,X}^{S_Y}(k) \quad \text{Eq. 3}$$

$$\varphi_X^{S_Y}(k) = D^{S_Y}(k) - I_X^{S_Y}(k) + MP_{\varphi,X}^{S_Y}(k) + n_{\varphi,X}^{S_Y}(k) + b_{\varphi,X}^{S_Y}(k) + \lambda_X A_X^{S_Y} \quad \text{Eq. 4}$$

where

$$D^{S_Y}(k) = \rho^{S_Y}(k) + c\left(dT^{S_Y}(k) - dt^{S_Y}(k)\right) + T^{S_Y}(k)$$

It is well-known that the ionospheric term can be approximated, at the first order, by:

$$I_X^{S_Y}(k) = \frac{40.3 \cdot STEC^{S_Y}(k)}{f_X^2}$$

where

- $f_X$ is the signal's carrier frequency, and
- $STEC$ is the Slant Total Electron Content (TEC), which represents the TEC along the signal propagation path.

## REFERENCE IONOSPHERE ESTIMATION TECHNIQUE

As mentioned earlier, the reference ionosphere delay estimation technique is fully presented in [Julien et al, 2009] and is only briefly described here.

### Dual Frequency Measurements

The ionosphere delay estimation process uses dual-frequency ionosphere code and phase geometry-free combinations:

$$\kappa_{X_1,X_2}\left(P_{X_1}^{S_Y}(k) - P_{X_2}^{S_Y}(k)\right) = I_{X_1}^{S_Y}(k) + \kappa_{X_1,X_2}\left(MP_{P,X_1}^{S_Y}(k) + n_{P,X_1}^{S_Y}(k) + b_{P,X_1}^{S_Y}(k) - MP_{P,X_2}^{S_Y}(k) - n_{P,X_2}^{S_Y}(k) - b_{P,X_2}^{S_Y}(k)\right) \quad \text{Eq. 5}$$

In the case of an E5a and E5b combination, the coefficient $\kappa_{E5b,E5a}$ is equal to 19.9 when estimating the ionospheric delay at E5b. This means that all the tracking errors (due to multipath, noise, interference) and hardware biases are multiplied by 19.9 when estimating the ionospheric delay. It is quite clear that this is very detrimental when the code measurements are used to estimate $I_{E5b}^{S_Y}(k)$. It is then interesting to use carrier-phase measurements instead. In this case, the multiplication factor is not as problematic as the tracking errors are only at the cm level. However, in this case, a float ambiguity term has to be estimated as well, which can be difficult. Due to their intrinsic ambiguity term, the carrier phase measurements cannot, however, be used as such. This means that it is necessary to form a system with $2n$ observations ($n$ dual-frequency code measurements + $n$ dual-frequency carrier-phase pseudoranges) which contains $2n$ unknowns ($n$ ionospheric delays + $n$ float carrier-phase ambiguities). Such a system is problematic since the estimation of the carrier-phase ambiguities and ionospheric delays will be greatly based on the highly contaminated dual-frequency code measurements. Moreover, all code and phase measurements are not linked together, thus every time a new satellite appears, it will take time to estimate the associate carrier-phase ambiguity. The system will also likely take time to converge and might thus not be relevant for our purpose.

### Local Ionospheric Model

To reduce the complexity and convergence time of the above-mentioned system, it is possible to try to use a simple local ionospheric delay model that could link all the ionospheric delays associated with each visible satellite. This allows reducing the number of ionospheric parameters to estimate and link all the available measurements so that the carrier-phase ambiguity of an appearing satellite would be more easily estimated in one update. Modeling the local variations of the vertical ionospheric delay around the user to facilitate the estimation of the ionospheric

slant delay has been used for single-frequency (GPS L1 C/A) ionospheric estimation in [Lestarquit et al. 1997; Moreno et al., 1999] and has also been used for dual frequency GPS L1/L2 measurements in [Komjathy, 1997] in the context of Precise Point Positioning (PPP) using a network of reference stations. Both models assume that the ionospheric delays can be modeled using:

- A single layer ionospheric model that is such that each point of the layer equals the VTEC
- A local VTEC model that is such that the VTEC at any ionospheric pierce point (intersection between an assumed single-layer ionosphere and the signal path) can be modeled as a function of the VTEC at a specific reference point and a linear variation of this reference VTEC according to the difference in latitude and longitude between the pierce point and the reference position.
- A mapping function that maps the VTEC at the ionosphere pierce point into the ionosphere delay. A typical mapping function to transform the VTEC into an STEC is [Lestarquit et al, 1999]:

$$MF^{S_Y}(k) = \frac{1}{\sqrt{1 - \left(\frac{R_e cos\left(E^{S_Y}(k)\right)}{R_e + h_I}\right)^2}} \qquad \text{Eq. 6}$$

where

- $R_e$ is the Earth radius (6378.1363 km),
- $E$ is the satellite elevation (in rad), and
- $h_I$ is the height of the maximum TEC, which is also the height of the ionosphere layer when modeled as a single-layer.

Regarding the local VTEC model, two cases are found in the literature:

1. the case where the reference VTEC is estimated at the user zenith [Lestarquit et al. 1997; Moreno et al., 1999]. In this case, the model of the VTEC at the ionosphere pierce point is:

$$\widehat{VTEC}_p(k) = \begin{pmatrix} VTEC_u(k) \\ +\left(lat_u(k) - lat_p^{S_Y}(k)\right) \cdot g_{lat}(k) \\ +\left(long_u(k) - long_p^{S_Y}(k)\right) \cdot g_{long}(k) \end{pmatrix} \qquad \text{Eq. 7}$$

where

- $VTEC_u$ is the VTEC at the user's zenith,
- $g_{lat}\ and\ g_{long}$ are the latitudinal and longitudinal VTEC gradients,
- $lat_u\ and\ lat_p$ are the user and pierce point latitudes, and
- $long_u\ and\ long_p$ are the user and pierce point longitudes.

2. the case where the reference VTEC is a fictitious point with the same latitude as the user and the same longitude as the mean sun longitude [Komjathy, 1997]. The reason for this model is to consider that the VTEC at the mean sun longitude is more stable (and thus easier to estimate) than the VTEC at the user's zenith, which can vary greatly. However, this model can only be used if a worldwide network of stations is used. This model is thus discarded in this report.

From the above, the ionospheric delay at frequency $X_1$ for satellite $S_Y$ can then be modeled as:

$$\hat{I}_X^{S_Y}(k) = \Big(I_{V,X,u}(k) + \Delta lat^{S_Y}(k) G_{X,lat}(k) + \Delta long^{S_Y}(k) G_{X,long}(k)\Big) \qquad \text{Eq. 8}$$

where

- $I_{V,X,u} = 40.3 \cdot MF^{S_Y} \cdot \frac{VTEC_{user}}{f^2}$
- $G_{L_1,lat} = 40.3 \cdot MF^{S_Y} \cdot g_{lat}$
- $G_{L_1,long} = 40.3 \cdot MF^{S_Y} \cdot g_{long}$
- $\Delta lat_{u,p}^{S_Y}(k) = lat_u(k) - lat_p(k)$
- $\Delta long_{u,p}^{S_Y}(k) = long_u(k) - long_p(k)$

**Ionosphere Estimation Kalman Filter**

The ionospheric delay estimation described in [Julien et al, 2009] is based on a Kalman filter in order to estimate the local VTEC model parameters as well as the carrier-phase ambiguities. The state matrix is directly linked to Eq. 5 and its carrier phase counter-part, and to the local ionosphere models presented earlier. It can be written as:

$$\begin{bmatrix} \Delta P_{E5a,E5b}^{S_1}(k) \\ \Delta P_{E5a,E5b}^{S_2}(k) \\ \cdots \\ \Delta P_{E5a,E5b}^{S_n}(k) \\ \Delta \varphi_{E5b,E5a}^{S_1}(k) \\ \Delta \varphi_{E5b,E5a}^{S_2}(k) \\ \cdots \\ \Delta \varphi_{E5b,E5a}^{S_n}(k) \end{bmatrix} = H \begin{bmatrix} VTEC_u(k) \\ g_{lat}(k) \\ g_{long}(k) \\ A_{E5b,E5a}^{S_1} \\ A_{E5b,E5a}^{S_2} \\ \cdots \\ A_{E5b,E5a}^{S_n} \end{bmatrix} + \begin{bmatrix} N_{P,E5a,E5b}^{S_1}(k) \\ N_{P,E5a,E5b}^{S_2}(k) \\ \cdots \\ N_{P,E5a,E5b}^{S_n}(k) \\ N_{\varphi,E5a,E5b}^{S_1}(k) \\ N_{\varphi,E5a,E5b}^{S_2}(k) \\ \cdots \\ N_{\varphi,E5a,E5b}^{S_n}(k) \end{bmatrix}$$

with

$$H = \frac{1}{\kappa_{E5a,E5b}} \begin{bmatrix} \bar{\bar{K}}_X(k) & \overline{\overline{\Delta lat}}(k) & \overline{\overline{\Delta long}}(k) & \bar{\bar{0}}_n \\ \bar{\bar{K}}_X(k) & \overline{\overline{\Delta lat}}(k) & \overline{\overline{\Delta long}}(k) & \kappa_{E5a,E5b} \bar{\bar{I}}_n \end{bmatrix}$$

where

- $\bar{\bar{K}}_X(k) = \begin{bmatrix} K^{S_1}(k) \\ K^{S_2}(k) \\ \dots \\ K^{S_n}(k) \end{bmatrix}$,
- $\overline{\overline{\Delta lat}}\ (k) = \begin{bmatrix} \Delta lat^{S_1}(k) \\ \Delta lat^{S_2}(k) \\ \dots \\ \Delta lat^{S_n}(k) \end{bmatrix}$,
- $\overline{\overline{\Delta long}}\ (k) = \begin{bmatrix} \Delta long^{S_1}(k) \\ \Delta long^{S_2}(k) \\ \dots \\ \Delta long^{S_n}(k) \end{bmatrix}$,
- $\bar{\bar{0}}_n$ is a n-by-n zero matrix
- $\bar{\bar{I}}_n$ is a n-by-n identity matrix
- $K^{S_Y}(k) = \frac{40.3}{\sqrt{1-\left(\frac{R_e \cos\left(E^{S_Y}(k)\right)}{R_e+h_I}\right)^2}}$
- $\Delta P^{S_Y}_{E5a,E5b} = P^{S_Y}_{E5a} - P^{S_Y}_{E5b}$
- $\Delta\varphi^{S_Y}_{E5b,E5a} = \varphi^{S_Y}_{E5b} - \varphi^{S_Y}_{E5a}$
- $A^{S_1}_{E5b,E5a} = \lambda_{E5b} A^{S_Y}_{E5b} - \lambda_{E5a} A^{S_Y}_{E5a}$
- $N^{S_1}_{P,E5a,E5b}$ and $N^{S_1}_{\varphi,E5a,E5b}$ are the observation noise assumed Gaussian.

The transition matrix is based on the following assumptions:

- The ionosphere-related terms are modeled as first-order Gauss-Markov processes with an infinite correlation time.
- The Earth rotation is taken into account to update the vertical ionospheric delay between 2 consecutive time updates.

The transition matrix associated to the reference local ionosphere model is thus:

$$\begin{bmatrix} VTEC_u(k+1) \\ g_{lat}(k+1) \\ g_{long}(k+1) \\ A^{S_1}_{E5a,E5b}(k+1) \\ A^{S_2}_{E5a,E5b}(k+1) \\ \dots \\ A^{S_n}_{E5a,E5b}(k+1) \end{bmatrix} = F \begin{bmatrix} VTEC_u(k) \\ g_{lat}(k) \\ g_{long}(k) \\ A^{S_1}_{E5a,E5b}(k) \\ A^{S_2}_{E5a,E5b}(k) \\ \dots \\ A^{S_n}_{E5a,E5b}(k) \end{bmatrix} + \begin{bmatrix} \sigma_{VTEC} \cdot n_{VTEC} \\ \sigma_{G_{lat}} \cdot n_{G_{lat}} \\ \sigma_{G_{long}} \cdot n_{G_{long}} \\ 0 \\ 0 \\ \dots \\ 0 \end{bmatrix}$$

with

$$F = \begin{bmatrix} 1 & 0 & W_e & 0 & \dots & 0 \\ 0 & 1 & 0 & 0 & \dots & 0 \\ 0 & 0 & 1 & 0 & \dots & 0 \\ 0 & 0 & 0 & 1 & \dots & 0 \\ \dots & \dots & \dots & \dots & \dots & 0 \\ 0 & 0 & 0 & 0 & 0 & 1 \end{bmatrix}$$

where

- $\sigma_{VTEC}$, $\sigma_{G_{lat}}$, $\sigma_{G_{long}}$ are the standard deviations associated with the uncertainty of the model,
- $n_{VTEC}$, $n_{G_{lat}}$, $n_{G_{long}}$ are independent Gaussian noise with a unit variance, and
- $W_e$ is the Earth rotation rate (rad/s)

It is interesting to note that this method has the advantage to separate the inter-frequency bias from the ionospheric delay estimation since the bias will be absorbed by the (float) ambiguity state once the filter has converged.

## ANALYSIS OF THE LOCAL IONOSPHERIC VARIATIONS USING NEQUICK AND DEDUCED LOCAL VTEC MODELS

Results presented in [Julien et al, 2009] showed, using simulations, that the ionosphere estimation filter presented earlier was suitable when the true ionosphere was assumed well represented by the Klobuchar model. These results were seen as overly optimistic as it is well known that the Klobuchar model does not represent well the true local variations of ionosphere. Moreover, the Klobuchar model is by nature fairly close to the local VTEC model. It was thus decided to model the true ionosphere using the NeQuick model. The description of the NeQuick model will not be given here. The main reasons for using it instead of the well-known Klobuchar model are the following:

- it is based on a realistic model of the true ionosphere since it uses a 4D model (latitude, longitude, altitude and time) that is based on the division of the ionosphere in several thick layers.
- it is valid worldwide, while the Klobuchar model is only valid at mid-latitude and for satellites with an elevation greater than 20°.
- It is generally recognized that the TEC values derived from the NeQuick model is representative of the true TEC values with an RMS error of around 20%, while it is only around 50% for the TEC values derived from the Klobuchar model.

For more information, please consult [Radicella et al, 1995]. Note that the following analysis uses the NeQuick model freely available on the ITU website [ITU] and that a recent evolution of this model (NeQuick 2) exists (although not used here).

Following this choice, it was decided to realize an early investigation of the typical behavior of the VTEC based on the NeQuick model. For this analysis, the variation of the VTEC in July 1990 is used. It represents an active ionosphere, but the analysis of other months confirm the results. The

drawback of the following VTEC analysis is that it uses the ITU R12 data, provided with the NeQuick model, as single input. There is only one R12 value per month, which means that they represent an average behavior of the VTEC. It is still believed that they represent general variations of the ionospheric delay over time.

Figure 1 represents the worldwide vertical ionospheric delay at L1 every 6 hours over 24 hours in July 1990. It can be clearly seen that according to the location of the user, the local VTEC does not change in the same way in the mid and lower latitudes.

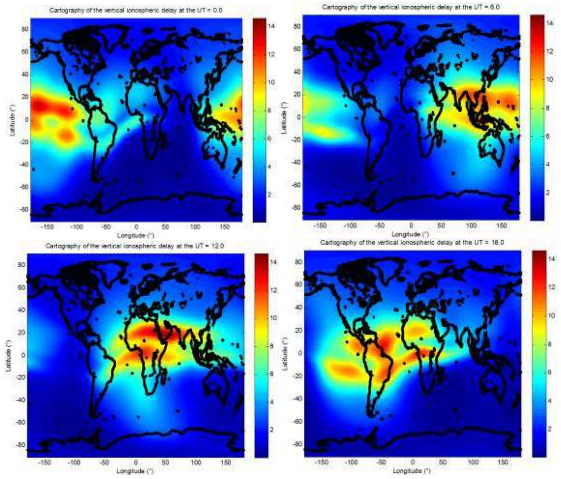

**Figure 1 - Vertical Ionospheric Delay at L1 as a mean day in July 1990 at UTC 0h, 6h, 12h and 18h**

In the mid latitude, the variation of the VTEC is fairly smooth, and the variation seems dominant in the North-South direction with slight variations when the VTEC peak passes close to the considered area (generally in the Northern hemisphere, the main variation of the VTEC is first in the South East/North West direction as the solar peak arrives from the East and then moves towards the South West/North East as the VTEC peak moves to the West direction). In general, a linear modeling of the VTEC, on the same basis as the one shown in Eq. 7, could appear appropriate. However, it seems that an interesting modification of this model would be to have an evolving coordinate system that would, at each epcoh, be the most appropriate to represent a linear variation of the vertical ionospheric delay (and thus would not constantly be in the North/South, East/West direction). As an example of mid-latitude phenomenon, it is possible to look at the variation of the vertical ionospheric delay around Toulouse, France. Figure 2 represents (1) the variation of the VTEC as a function of the latitude assuming a constant longitude that is that of Toulouse, and (2) the variation of the VTEC as a function of the longitude assuming a constant latitude that is that of Toulouse. It can be seen that in July 1990, the variation is fairly linear as a function of the longitude. However, it appears more like a 2nd order polynomial function as a function of the latitude. This was strongly confirmed doing the same analysis in Sevilla, Los Angeles, Sydney and Johannesburg (where even a 2nd order polynomial would not appear appropriate).

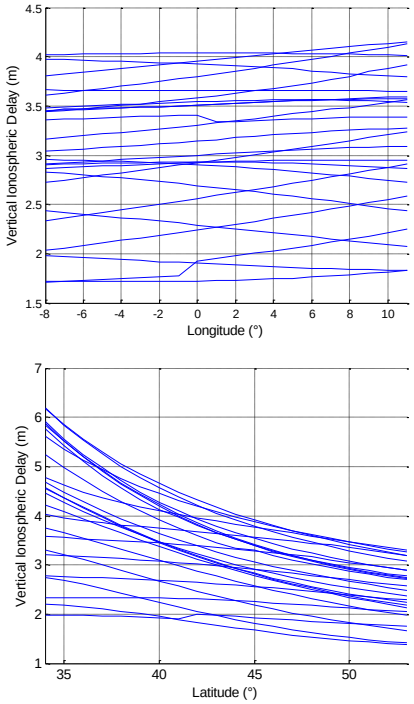


**Figure 2 - Representation of the Vertical Ionospheric Delay over 24 hours as a Function of the Longitude for a Constant Latitude - that of Toulouse - (Left) and as a Function of the Latitude for a Constant Longitude - that of Toulouse - (Right)**

In the lower latitudes, the variation of the TEC is very different. Indeed, in this zone the maximum peak of vertical ionospheric delay is present. In July 1990, two VTEC peaks (one around +20° and one around -20° with respect to the magnetic equator) are present. As a consequence, it is clear that when the VTEC peaks pass close or within the area where the pierce points are located, the variation will not be linear anymore since the vertical TEC will decrease in all directions around the VTEC maximum. It is even worse in locations that are between the VTEC peaks. In this case, a more advanced estimation technique should be used (that has to be much more advanced than just a linear model).

This analysis has been realized on a limited number of places and in a month during which the ionosphere activity was particularly intense due to the solar peak. Still, it shows that in the considered conditions, the estimation of the ionospheric delay based on a linear model will be difficult, especially in the low latitudes. In the mid latitudes, a linear model appears more appropriate although not always appropriate, especially in the North/South direction. In the following, only the European region will be analyzed.

Finally, it has to be mentioned that this analysis only looked at the vertical ionospheric delay. Another source of error when using the models presented in Eq. 6 is the assumption that the mapping function is very accurate. This is a very strong assumption considering that the electron density of the ionosphere layers will play a different role depending if the user is close to an ionospheric peak or not.

**Selected Local VTEC Models**

Based on the previous analysis, and on the ionosphere properties, 8 local VTEC models are proposed and analyzed to update the [Julien et al, 2009] estimation filter:

- the **first model** is the reference model already presented in Eq. 7.
- the **second model** aims at refining the first model by adding an extra degree of freedom that would represent a diagonal component. This model is:

$$\widehat{VTEC}_p(k) = \begin{pmatrix} VTEC_u(k) + \Delta lat_{u,p}^{S_Y}(k) \cdot g_{lat}(k) \\ +\Delta long_{u,p}^{S_Y}(k) \cdot g_{long}(k) \\ +\Delta lat_{u,p}^{S_Y}(k) \cdot \Delta long_{u,p}^{S_Y}(k) \cdot g_{lat,long}(k) \end{pmatrix} \quad \text{Eq. 9}$$

  where $g_{lat,long}$ is a new gradient term representing the variation of the VTEC in the diagonal direction with respect to the North/South and East/West directions.
- the **third model** aims at taking into account the fact the VTEC variation in the North/South direction appears more like a second order variation (see Figure 2 for instance). This third model is:

$$\widehat{VTEC}_p(k) = \begin{pmatrix} VTEC_u(k) + \Delta lat_{u,p}^{S_Y}(k) \cdot g_{lat}(k) \\ +\left(\Delta lat_{u,p}^{S_Y}(k)\right)^2 \cdot g_{lat2}(k) \\ +\Delta long_{u,p}^{S_Y}(k) \cdot g_{long}(k) \end{pmatrix} \quad \text{Eq. 10}$$

  where $g_{lat2}$ is a new gradient term representing the second order variation of the VTEC in the North/South direction.
- the **fourth model** aims at refining the reference model by adding two extra degrees of freedom by fully separating the gradients in the East, West, South and North directions. The resulting local VTEC model is:

$$\widehat{VTEC}_p(k) = \begin{pmatrix} VTEC_u(k) + max\left(\Delta lat_{u,p}^{S_Y}(k), 0\right) \cdot g_{lat,pos}(k) \\ +min\left(\Delta lat_{u,p}^{S_Y}(k), 0\right) \cdot g_{lat,neg}(k) \\ +max\left(\Delta long_{u,p}^{S_Y}(k), 0\right) \cdot g_{long,pos}(k) \\ +min\left(\Delta long_{u,p}^{S_Y}(k), 0\right) \cdot g_{long,min}(k) \end{pmatrix} \quad \text{Eq.11}$$

  where
  - $g_{lat,pos}$ and $g_{lat,neg}$ represent the latitudinal gradients when the latitude of the user is greater and lower than that of the pierce point, respectively, and
  - $g_{long,pos}$ and $g_{long,neg}$ represent the longitudinal gradients when the longitude of the user is greater and lower than that of the pierce point, respectively.
- the **fifth model** is directly based on the fourth model with the difference that the coordinates used in the model correspond to a different frame. Instead of the latitude/longitude coordinated, the coordinate system will be based upon the following rotating axes:
  - the x-axis is aligned with the line going from the user and the assumed VTEC peak location. In the following analysis, this VTEC peak location will be assumed to be located at a latitude that is 20° above the magnetic equator and at a longitude that is the longitude of the orthogonal projection of the sun on the Earth surface.
  - the y-axis is perpendicular to the x-axis. This means that the latitudes and longitudes of the ionospheric pierce points will have to be rotated continuously.
- The **sixth model** is the same model as the reference model, with the exception that the latitude of the ionospheric pierce points are expressed as magnetic latitudes (Dip). The grounds for this model is that the NeQuick uses the Dip latitudes to compute the VTEC.
- The **seventh model** is a combination of the sixth model and the fourth model. The pierce points' latitudes are expressed as magnetic latitudes, and the variation of there are 4 VTEC gradients: one on each cardinal directions.
- The **eighth model** is the same as the seventh model, except that the pierce points' latitudes are expressed as modified dip latitudes. The grounds

for this model is that the NeQuick uses also the modified Dip latitudes to compute the VTEC.

These models can be included in a straightforward manner in the Kalman filter presented for the reference model.

## PRESENTATION OF THE SIMULATION TOOL AND FILTER SETTINGS

### Simulation Tool

The simulation tool is exactly the same as the one used in [Julien et al, 2009]. The only difference being that the true ionosphere is now modeled using the NeQuick model instead of the Klobuchar model. For visualization purpose, the $C/N_0$ for the considered signal's component at the user antenna output is shown in Figure 3**Erreur ! Source du renvoi introuvable.**.

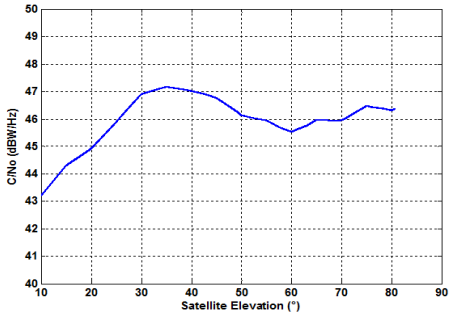


**Figure 3 – $C/N_0$ at the Antenna Output**

### Kalman Filter Settings

The observation noise variance was chosen to be the product of a $C/N_0$-dependent term and an elevation-dependant term. The $C/N_0$-dependent term is the usual theoretical tracking noise variance. The elevation-dependent variance represents the impact of multipath and was chosen to be $\frac{1}{4}\left(3+\frac{1}{\sin\left(E^{SV}(k)\right)}\right)$.

Note that the system has to deal with a changing number of measurements (appearing and disappearing satellites). The initial state value is approximated thanks to the use of the Klobuchar model, assuming that the latitudinal and longitudinal gradients are zero.

The chosen covariance matrix of the state transition model was set empirically to allow for a variation of 0.1 cm/s for the vertical ionosphere component and 0.5 cm/rad/s for the gradients.

In the presented Kalman filter, the carrier-phase ambiguity term is satellite-dependent, which means that this state will tend to absorb all the errors that are not common to the different carrier-phase observations. By assuming that the ambiguities are fixed (their state's variance equals 0), the residual ionospheric delay model error will not be absorbed (or over a very long time) by the ambiguity states, except for a potential bias during the initial convergence period of the filter. This might create a bias in the estimation process. In order to limit this effect, it was decided to consider that the ambiguity state was not completely constant. Instead, it was decided to consider it as a first-order Markov process with a medium correlation time (explored later on) in order for the ambiguity state to still absorb the ionospheric delay model error, thus improving the adaptability of the filter to the changing ionosphere activity. As a first approximation, the correlation time of the ambiguity state will be considered equal for all ambiguity states.

To test the different local VTEC models, 3 locations were selected to represent a diversity in terms of latitude in Europe:

- **Sevilla** (37.418056°N, 5.898889°W), which is supposed to be closer to the VTEC peak and should thus have higher VTEC gradients
- **Toulouse** (43.6170°N, 1.4500°E), which is in the middle of Europe (in terms of latitude) and should have average VTEC gradients, and
- **Stockholm** (59.651944°N, 17.918611°E), which is in the upper part of Europe (in terms of latitude) and should have low VTEC gradients

Also, two periods of time were taken to represent the TEC during a high to very high ionosphere activity. These periods were selected thanks to the table of R12 parameters over the period 1931-2001 provided by ITU. The two periods selected were:

- **January 1990**, it has a very high R12 value (150.6), representing a very active ionosphere (92.5% of all the R12 values in the ITU table are lower than 150.6), and
- **January 2001**. it has a high R12 value (108.7), representing an active ionosphere (73.7% of all the R12 values in the ITU table are lower than 150.6).

Four figures of merit are analyzed:

- the mean ionosphere estimation error at L1,
- the 68$^{th}$ percentile of the ionosphere estimation error at L1
- the 95$^{th}$ percentile of the ionosphere estimation error at L1

- the 99th percentile of the ionosphere estimation error at L1

The ionospheric delay at L1 in Toulouse in January 1990 is represented as a function of time and satellite elevation in Figure 4.

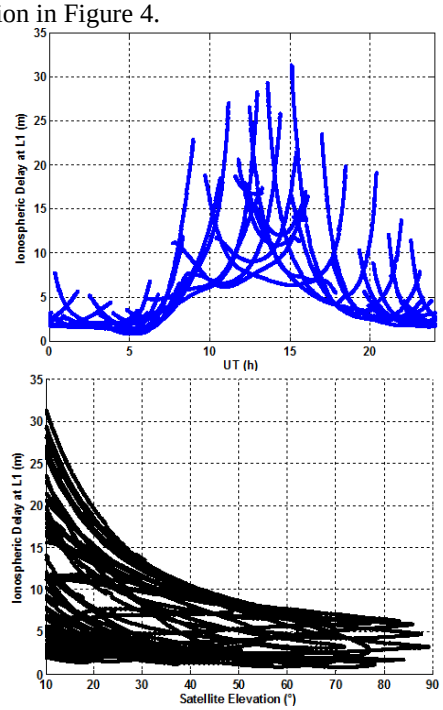


**Figure 4 - Ionosphere Delay at L1 as a Function of Time and Satellite Elevation in Toulouse in January 1990**

## TESTS WITH THE REFERENCE MODEL

Initial tests were realized using only the reference model. These tests were meant to understand and set a few number of parameters: the ambiguity state's variance, the assumed ionospheric height shell, and the receiver mask angle.

### Impact of Ambiguity States' Variance

The first series of tests were designed to test the sensitivity of the estimation process with respect to the variance associated to the ambiguity state in the transition matrix. This was tested for 4 different values of the standard deviation of the ambiguity states in the transition matrix: 0 mm/s, 0.01mm/s, 0.1mm/s and 1mm/s. The results are provided in Table 1 for Toulouse (as an example). It can be seen that the use of a non-zero variance for the ambiguity states in the transition matrix improves significantly the estimation process. It can also be seen that the best results are achieved for an ambiguity state's standard deviation equal to 1 mm/s for Toulouse when the ionosphere activity is very high (Jan 1990). This is similar for Sevilla, but differs for Stockholm where a value of 0.1 mm/s seems optimal for Jan 1990. A value of 0.1 mm/s also appears optimal for Toulouse and Sevilla in 2001 during more stable ionosphere conditions. This is in line with the fact that it is preferable if these states could absorb part of the ionosphere model estimation error: the magnitude of the optimal standard deviation of the ambiguity states is dependent upon the variation of the ionospheric delay compared to the proposed model.

**Table 1 - Sensitivity Analysis of the Ionospheric Delay Estimation Process wrt the Ambiguity States' Standard Deviation**

| Ambiguity States' Standard Deviation (mm/s) | | Toulouse | |
|---|---|---|---|
| | | 1990 | 2001 |
| **0** | Mean | -0.3 | -0.24 |
| | 68 percentile | 0.63 | 0.46 |
| | 95 percentile | 2.59 | 1.42 |
| | 99 percentile | 6.22 | 2.54 |
| **0.01** | Mean | 0.00 | -0.17 |
| | 68 percentile | **0.47** | 0.36 |
| | 95 percentile | 1.87 | **0.79** |
| | 99 percentile | 3.72 | 1.64 |
| **0.1** | Mean | 0.10 | 0.09 |
| | 68 percentile | **0.47** | **0.29** |
| | 95 percentile | 1.58 | 0.90 |
| | 99 percentile | 3.13 | **1.57** |
| **1** | Mean | 0.06 | 0.10 |
| | 68 percentile | **0.43** | **0.34** |
| | 95 percentile | **1.47** | 0.99 |
| | 99 percentile | **2.53** | 1.68 |

Note: Bold values are the lowest values per city and year within 5 cms.

Several other results are interesting from these tests.

- Even during an intense solar activity (Jan 1990), the estimation procession seems fairly good in Stockholm, while it is significantly more difficult in Toulouse and extremely difficult in Seville. This is normal since the VTEC close to polar regions (assuming nominal behavior of the ionosphere) is much less affected than in middle latitude regions.
- Sevilla, which is the southern-most city of the 3 test cities is much more affected by the solar activity than Toulouse and Stockholm during high solar activity. This clearly impacts the ionospheric delay estimation process which is

much worse in January 1990 in Seville than in Toulouse.

- During medium solar activity, the ionospheric delay estimation is more or less the same in Toulouse and Stockholm, and significantly worse in Sevilla

An example of the ionospheric delay estimation error, estimated vertical ionosphere delay and estimated latitudinal and longitudinal gradients (all at L1) in Toulouse in January 1990 are represented in Figure 5.

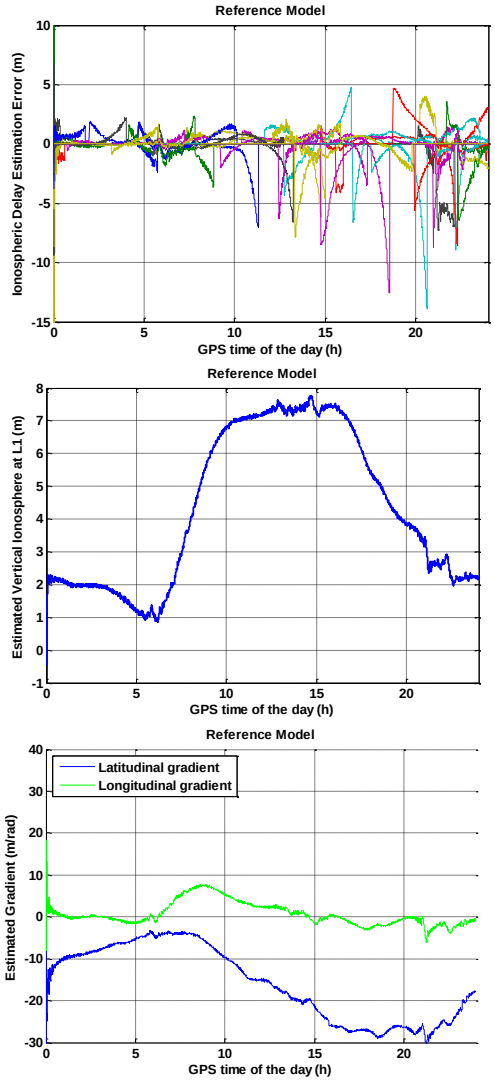


**Figure 5 - Ionospheric Delay Estimation Error at L1 (Top), Estimated Vertical Ionosphere Delay at L1 (Middle) and Estimated Latitudinal and Longitudinal Gradients at L1 (Bottom) in Sevilla in January 1990 (Ambiguity States' Standard Deviation is equal to 1 mm/s)**

**Impact of the Assumed Ionosphere Shell Height**

A series of tests was conducted to test the sensitivity of the estimation process with respect to the height of the assumed ionosphere shell. Because the estimation model relies on a thin shell model, the assumed height of the ionospheric shell impacts the location of the pierce points, the mapping function (Eq. 7), and thus the estimation process. It appears that the best performance when the solar activity is high is for an ionosphere shell height equal to 300 km, while the best performance when the solar activity is medium is for an ionosphere shell height equal to 400 km. Because the usual assumed ionospheric shell height is generally 350 km (Klobuchar model), this value will be kept in the following.

**Impact of the Receiver Mask Angle**

The last series of tests was meant to see how the ionosphere estimation process improves as a function of the receiver mask angle. To do this, 2 situations were tested, both looking at the estimation error statistics for satellites above 20°:

- the case when the receiver mask angle is 10°, and
- the case when the receiver mask angle is 20°.

It was observed that the results were better when the receiver mask angle is 20° for Toulouse and Sevilla in both considered periods of time. However, it is the opposite for Stockholm. This makes sense since in Toulouse and Sevilla, where the true ionosphere delay fluctuates more, the error brought by low elevation satellite is greater, due to the high ionospheric delay variation, and probably corrupts the estimation process.

## PERFORMANCE OF THE PROPOSED VTEC MODELS

In the following, the 7 other models presented earlier are tested against the reference model. Table 4 (at the very end of the paper) shows the results for Sevilla, Stockholm and Toulouse in January 1990 and January 2001. The settings for the simulations were a receiver mask angle of 10°, an assumed ionosphere shell height of 350 km, and an ambiguity states' standard deviation of 0.1 mm/s.

Regarding Toulouse and Sevilla, it appears that the 7th model (use of dip latitudes associated with 4 independent VTEC gradients) gives the best overall performance. The estimated ionospheric delay error, estimated vertical ionospheric delay and North, East, South and West gradients in Toulouse in January 1990 are presented in Figure 6. It can be seen that during the whole simulation, the East and West

gradients are remaining close, indicating that the gradient in the East/West direction is indeed close to linear. On the other hand, it can be seen that the North and South gradients begin to be significantly different after 12:00, which is when the VTEC peak approaches the South of Toulouse. It then makes sense to dissociate the North and South gradients.

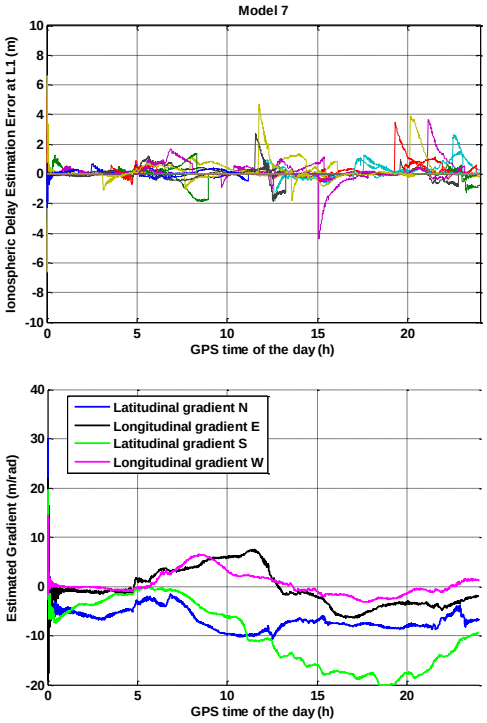


**Figure 6 - Ionospheric Delay Estimation Error at L1 (Top), and Estimated Latitudinal and Longitudinal Gradients at L1 (Bottom) in Toulouse in January 2001 using Model 7 (Ambiguity States' Standard Deviation is equal to 0.1 mm/s)**

Regarding Stockholm, the results are once again different due to the lower variation of the ionospheric delay over time and space. The local VTEC models providing the best ionosphere delay estimation appears to be:

- the reference model and the 2nd model (with diagonal component) for the high ionosphere activity case (1990), and
- the reference model, the 2nd model (with a diagonal component) and the 6th model (dip latitudes) for the low ionosphere activity case (2001).

As a conclusion, comparing the best resulting using the 7th model for Toulouse and Sevilla, and the reference model for Stockholm, it can be seen that the best results are obtained for Stockholm, then Toulouse, and finally Sevilla, as expected. The best performances are gathered in Table 2 for a receiver mask angle of 10° and in Table 3 for a receiver mask angle of 20°.

**Table 2 - Performance Analysis of the Ionospheric Delay Estimation Process for the Selected Models (Receiver Mask Angle of 10°)**

| | Toulouse | | Sevilla | | Stockholm | |
|---|---|---|---|---|---|---|
| | **1990** | **2001** | **1990** | **2001** | **1990** | **2001** |
| **Mean** | 0.14 | 0.09 | 0.11 | 0.04 | -0.04 | -0.06 |
| **68%** | 0.32 | 0.24 | 0.40 | 0.27 | 0.35 | 0.30 |
| **95%** | 1.16 | 0.75 | 1.95 | 0.87 | 1.16 | 1.00 |
| **99%** | 2.45 | 1.34 | 4.27 | 1.72 | 2.05 | 1.79 |
| **Max** | 4.67 | 3.16 | 9.02 | 3.05 | 3.22 | 3.02 |

**Table 3 - Performance Analysis of the Ionospheric Delay Estimation Process for the Selected Models (Receiver Mask Angle 20°)**

| | Toulouse | | Sevilla | | Stockholm | |
|---|---|---|---|---|---|---|
| | **1990** | **2001** | **1990** | **2001** | **1990** | **2001** |
| **Mean** | 0.07 | 0.05 | 0.03 | 0.00 | 0.04 | 0.02 |
| **68%** | 0.25 | 0.18 | 0.30 | 0.19 | 0.22 | 0.20 |
| **95%** | 0.73 | 0.52 | 0.94 | 0.51 | 0.70 | 0.58 |
| **99%** | 1.17 | 0.74 | 1.85 | 0.86 | 0.95 | 0.81 |
| **Max** | 3.06 | 1.18 | 3.86 | 1.38 | 1.53 | 1.62 |

**Performance of the selected Models over the Year**

For the last series of tests, it was decided to have results for several months within the same year in order to make sure that the previous analysis, based on the month of January, was representative. The simulations were done for a user in Toulouse during 4 different months of the year: January, April, July and October. The tests are made for both years 1990 and 2001. The selected ionospheric delay estimation models is the 7th model (dip latitude + 4-axis gradients), and the settings are:

- ambiguity states' standard deviation: 0.1 mm/s,
- assumed ionospheric shell height: 350 km, and
- mask angle: 10°.

The results are shown in Figure 7. It can be seen that January appears to be a 'difficult' month compared to April and July, while October is the month that leads to the strongest estimation errors. This is true for both the 1990 and 2001 years. It must be inherent to the NeQuick model. It can be seen that all over the year, 68% of the ionospheric delay estimation error at L1 is lower than 0.4m in 1990 and 0.31m in 2001. On the

other hand, the maximum estimation error at L1 can be very high (5.39m in 1990 and 3.33 in 2001)

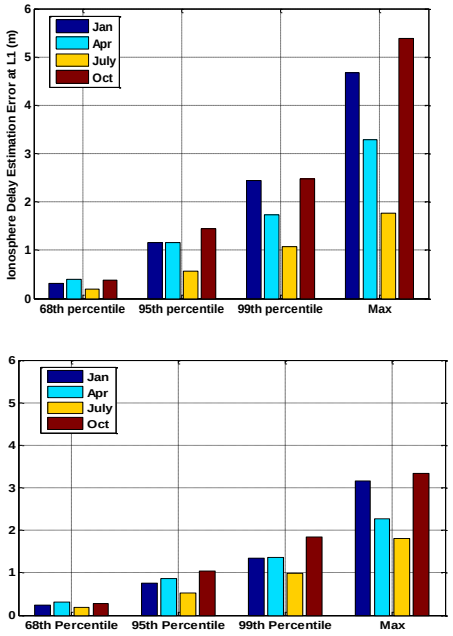


**Figure 7 - Ionospheric Estimation Results in Toulouse in January, April, July and October of 1990 (Top) and 2001 (Bottom)**

## CONCLUSIONS AND FUTURE WORK

### Conclusions

This study has showed the need to use a more advanced model than the Klobuchar model to represent the ionospheric delay variation. For this purpose, the NeQuick model was used as it is recognized to be much more representative of the ionosphere TEC.

The use of the NeQuick model showed that the VTEC variations over Europe could be significantly different between Northern and Southern Europe. In Southern Europe, the VTEC can vary significantly since it is close to the passing VTEC hot spot. On the other hand, the VTEC variations in Northern Europe are milder.

The estimation of the ionospheric delay associated to each satellite was estimated thanks to a Kalman filter that uses the code and carrier-phase dual frequency measurements, and a simplified ionospheric delay model based on:

- a thin shell ionospheric model
- a mapping function dependent upon the ionosphere shell height and the satellite elevation
- a local VTEC model in order to estimate the VTEC values at the ionospheric pierce point. This local VTEC map was based on the VTEC above the user and gradients in different directions.

A total of 8 local VTEC models were tested to take into account the specificities of the VTEC variations over Europe.

The first finding of this investigation was regarding the Kalman filter design. Indeed, it was shown that it was extremely important to design the filter so that it allows a variation of the carrier-phase ambiguity state. By doing so, the filter better adapts to the variation of the VTEC modeling errors. This greatly reduces the ionospheric delay estimation error.

It was shown that the most appropriate local VTEC model for Southern and Central Europe was a model with 5 states: the estimated vertical ionospheric delay above the user, and 4 gradients in the 4 cardinal directions. This model also used geomagnetic latitudes (dip) instead of true latitude. This model particularly showed the relevance of using an independent gradient in the North and South directions with respect to the user location. Indeed, when the VTEC maximum passes close to the user location, there can be very high non-linear variations of the VTEC in this direction.

Regarding Northern Europe, a simpler model could be used as the VTEC variation is much milder. the proposed VTEC model is composed of only 3 states: the vertical ionospheric delay above the user and 2 gradients: 1 in the North/South direction, and 1 in the East/West direction. Although simpler, this model takes advantage of a greater observability of these states. This appears to be the winning choice, as the VTEC variations are not very strong.

Different solutions should thus be envisaged according to the user location with respect to the VTEC hot spot.

Simulations showed that in Toulouse, under a particularly active ionosphere (in the top 7.5% over the 1931-2001 period):

- for satellites above an elevation of 20°:
  - The ionospheric delay estimation at L1 is below 30cm 68% of the time.
  - The ionospheric delay estimation at L1 is below 150cm 99% of the time.
- for satellites above an elevation of 10°:

- The ionospheric delay estimation at L1 is below 50cm 68% of the time.
- The ionospheric delay estimation at L1 is below 250cm 99% of the time.

**Future Work**

Several improvements/consolidations can be envisaged for the proposed technique:

- the simulations should be run using the new updated NeQuick model (NeQuick 2) as the model for the true ionospheric delay,
- a local VTEC model based on 3 gradients: East/West, North and South could be tested as it seems a good compromise between complexity and state observability. This new model comes from the fact that the North/South variations of the VTEC are much greater than in the East/West direction
- the proposed estimation method should be tested more extensively within and outside Europe
- The simulations should be run using a more representative multipath model, as the one used in the present simulations was based on a single reflection coming from the ground.

**REFERENCES**


European Union, (2010), *European GNSS (Galileo) Open Service Signal-in-Space Interface Control Document*.

Issler, J-L., Ries, L., Bourgeade, J-M., Lestarquit, L., Macabiau, C. (2004), Probabilistic Approach of Frequency Diversity as Interference Mitigation Means, Proceedings of the 2004 ION International Technical Meeting (Long Beach, Sept. 21-24).

ITU-R (1997), *Reference ionosphere characteristics*, *Recommendation P.1239*. (approved in 1997-05, managed by ITU-R Study Group SG3).

Julien O., Macabiau C., Issler J-L., L. Lestarquit (2009), *Ionospheric Delay Estimation Strategies Using Galileo E5 Signals Only*, Proceedings of the ION GNSS 2009, Savannah, GA, USA

Klobuchar John A. (1996), *Ionospheric effects on GPS*. [ed.] Bradford W. Parkinson and James J. Spilker Jr. Global Positioning Sytem : Theory and Applications. 1996, Vol. I, pp. 485-515.

Komjathy A (1997), *Global ionospheric Total Electron Content mapping using the Global Positioning System*. Departments of Geodesy and Geomatics Engineering, University of New Brunswick. Fredericton, New Brunswick, Canada : s.n., 1997. Ph.D. dissertation.

Leitinger, R., Zhang, M.L., Radicella, S.M., 2005. *An improved bottomside for the ionospheric electron density model NeQuick*, Annals of Geophysics 48 (3), 525–534.

Lestarquit, L. N. Suard, and J.-L. Issler (1997), *Determination of the Ionospheric Error using only L1 Frequency GPS Receiver*, Proceedings of the 1997 ION National Technical Meeting (Santa Monica, CA, Jan 14-16), pp. 313-322.

Moreno, R., N. Suard (1999), Ionospheric delay using only L1: validation and application to GPS receiver calibration and to inter-frequency biases estimation, Proceedings of the 1999 ION National Technical Meeting (San Diego, CA, Jan. 25-27), pp. 119-125.

Radicella, S.M. and M.L. Zhang (1995), *The improved DGR analytical model of electron density height profile and total electron content in the ionosphere*, Annals of Geophysics., Vol 38, No. 1.

Shau-Shiun Jan (2002), *Analysis of a Three-Frequency GPS/WAAS Receiver to Land an Airplane*, Proceedings of the ION National Technical Meeting (2002).

Simski, A, J.-M. Sleewaegen, M. Hollreiser, and M. Crisci (2006), *Performance Assessment of Galileo Ranging Signals Transmitted by GSTB-V2 Satellites*, Proceedings of the 1992 Institute Of Navigation GPS Conference (Albuquerque, NM, Sept. 16-18), pp. 483-490.

**Table 4 - Performance Analysis of the Ionospheric Delay Estimation Process using the 8 Local Ionosphere Models (for an Assumed Ionospheric Shell Height of 350 km, an Ambiguity States' Standard Deviation of 0.1 mm/s, and a Receiver Mask Angle Equal to 10°)**

| | | Toulouse | | Sevilla | | Stockholm | |
|---|---|---|---|---|---|---|---|
| | | **1990** | **2001** | **1990** | **2001** | **1990** | **2001** |
| **Reference Model** | Mean | 0.10 | 0.09 | 0.09 | 0.05 | -0.04 | -0.06 |
| | 68 percentile | 0.47 | **0.29** | 0.76 | 0.36 | **0.35** | **0.30** |
| | 95 percentile | 1.58 | 0.90 | 3.22 | 1.22 | **1.16** | **1.00** |
| | 99 percentile | 3.13 | 1.57 | 6.37 | 2.47 | **2.05** | 1.79 |
| | Max | 6.21 | 2.25 | 10.49 | 4.00 | **3.22** | 3.02 |
| **Model 2** | Mean | 0.12 | 0.09 | 0.12 | 0.07 | -0.02 | -0.05 |
| | 68 percentile | 0.46 | **0.29** | 0.75 | 0.34 | **0.34** | **0.30** |
| | 95 percentile | 1.57 | 0.90 | 3.08 | 1.17 | **1.19** | **1.05** |
| | 99 percentile | 2.91 | 1.48 | 5.99 | 2.49 | **2.10** | 1.86 |
| | Max | 6.17 | 2.32 | 9.53 | 3.62 | **3.25** | 3.14 |
| **Model 3** | Mean | 0.12 | 0.09 | 0.11 | 0.06 | -0.05 | -0.07 |
| | 68 percentile | 0.43 | **0.29** | 0.69 | **0.32** | **0.35** | 0.31 |
| | 95 percentile | 1.29 | 0.83 | 2.76 | 1.13 | 1.22 | 1.08 |
| | 99 percentile | 2.71 | 1.47 | 4.58 | 1.96 | 2.15 | 1.93 |
| | Max | 5.72 | 2.39 | **8.04** | 4.09 | 3.70 | 3.44 |
| **Model 4** | Mean | 0.17 | 0.11 | 0.17 | 0.07 | -0.07 | -0.09 |
| | 68 percentile | **0.35** | **0.25** | 0.57 | **0.33** | **0.31** | **0.26** |
| | 95 percentile | 1.31 | **0.79** | 2.42 | 1.08 | 1.23 | **1.05** |
| | 99 percentile | 2.67 | 1.44 | 4.76 | 1.82 | 2.53 | 2.23 |
| | Max | 5.15 | 3.37 | 10.35 | 4.31 | 4.74 | 4.45 |
| **Model 5** | Mean | 0.14 | 0.07 | 0.14 | 0.04 | -0.09 | -0.10 |
| | 68 percentile | 0.48 | **0.27** | 0.80 | 0.40 | **0.33** | **0.29** |
| | 95 percentile | 1.65 | 0.93 | 3.41 | 1.36 | 1.31 | 1.07 |
| | 99 percentile | 3.24 | 1.80 | 6.33 | 2.52 | 2.28 | 2.04 |
| | Max | 7.47 | 3.02 | 13.17 | 5.29 | 3.71 | 3.59 |
| **Model 6** | Mean | 0.07 | 0.08 | -0.02 | 0.00 | -0.01 | -0.04 |
| | 68 percentile | 0.40 | **0.29** | 0.59 | **0.30** | 0.37 | **0.32** |
| | 95 percentile | 1.39 | 0.84 | 2.79 | 0.97 | 1.32 | 1.10 |
| | 99 percentile | 2.60 | **1.38** | 5.40 | 2.18 | 2.12 | **1.66** |
| | Max | 5.26 | **2.11** | 9.04 | 3.78 | **3.26** | **2.96** |
| **Model 7** | Mean | 0.14 | 0.09 | 0.11 | 0.04 | -0.05 | -0.07 |
| | 68 percentile | **0.32** | **0.24** | **0.40** | **0.27** | **0.36** | **0.28** |
| | 95 percentile | **1.16** | **0.75** | **1.95** | **0.87** | 1.45 | 1.22 |
| | 99 percentile | **2.45** | **1.34** | **4.27** | 1.72 | 2.76 | 2.20 |
| | Max | **4.67** | 3.16 | 9.02 | **3.05** | 4.15 | 3.70 |
| **Model 8** | Mean | 0.15 | 0.09 | 0.11 | 0.04 | -0.05 | -0.07 |
| | 68 percentile | **0.33** | **0.24** | 0.47 | **0.28** | **0.36** | **0.28** |
| | 95 percentile | **1.18** | **0.77** | 2.12 | **0.91** | 1.42 | 1.18 |
| | 99 percentile | 2.65 | **1.36** | 4.51 | **1.66** | 2.75 | 2.19 |
| | Max | **4.67** | 3.19 | 8.76 | 3.24 | 4.29 | 3.84 |

Note: Bold values are the lowest values per city, year within 5 cms.